Journal of Applied Polymer Science

Intercalated polyaniline–kaolinite nanocomposite prepared via *in situ* mechanochemical synthesis

Hao Zheng,[1] Xue Feng,[1] Lu Zhou,[2] Ying Ye,[1] Jianfang Chen[3]

[1]Ocean College, Zhejiang University, Zhoushan 316021, People's Republic of China
[2]Department of Chemistry, Zhejiang University, Hangzhou 310027, People's Republic of China
[3]Key Laboratory of Marine Ecosystems and Biogeochemistry, Second Institute of Oceanography, State Oceanic Administration, Hangzhou 310012, People's Republic of China
Correspondence to: H. Zheng (E-mail: zhenghao@zju.edu.cn)

ABSTRACT: The *in situ* polymerization of aniline monomers within kaolinite interlayers easily led to an intercalated polyaniline (PANI)–kaolinite nanocomposite through a facile mechanochemical method. The X-ray diffraction results demonstrate that PANI was successfully intercalated in the interlayers of kaolinite, which was lightened by an increased basal spacing from 7.24 to 14.67 Å of kaolinite in the as-synthesized nanocomposite, and the characterization results from Fourier transform infrared spectrometry, scanning electron microscopy, transmission electron microscopy, and atomic force microscopy further confirm this conclusion. The thermal stability of PANI was improved significantly when PANI was intercalated into kaolinite to form the nanocomposite; this was proven by thermogravimetric analysis. Moreover, a panel experiment was carried out under a simulated marine environment to evaluate the anticorrosive effect of the as-prepared product, and the results show that the epoxy resin/intercalated PANI–kaolinite nanocomposite coating had a better anticorrosive effect than that of the neat epoxy resin coating. © 2016 Wiley Periodicals, Inc. J. Appl. Polym. Sci. **2016**, *133*, 43551.

KEYWORDS: clay; composites; conducting polymers; synthesis and processing; thermogravimetric analysis (TGA)

Received 17 November 2015; accepted 15 February 2016
DOI: 10.1002/app.43551

INTRODUCTION

In the past several decades, polyaniline (PANI) has attracted considerable attention because of its excellent comprehensive performance, including its better environmental stability, inexpensive raw materials, facile synthesis, and unique conductive mechanism.[1–4] An important application of PANI is in metal anticorrosion,[5–7] which refers to the painting of a composite coating containing PANI on the surface of a metal to protect the metal against corrosion. However, the thermal stability, mechanical properties, and adhesion of the pure PANI to the substrate are relatively poor; this significantly limits its applications in metal anticorrosion.

To improve the performance of PANI, various methods have been developed to modify PANI with inorganic additives such as clays.[8–10] It is well known that clays are very thermally stable with excellent mechanical properties and adhesion performance to the substrate, so the combination could achieve a synergistic effect. Moreover, some other properties of PANI could also be improved correspondingly. A common method involves the *in situ* oxidative polymerization of aniline monomers in aqueous solutions containing montmorillonite,[11] halloysite,[12] laponite,[13] palygorskite,[14] and attapulgite.[15] Another popular practice is to synthesis PANI-intercalated composites through intercalation techniques. Recently, many studies on intercalated polymer/montmorillonite composites have been performed[16–23] and have included changes in the spectroscopic properties of the PANI component and enhancements in the thermal stability and mechanical properties. However, studies on intercalated polymer–kaolinite composites have been relatively fewer, despite several reports on polymer–kaolinite hybrid composites.[24,25] The reasons for this are described in detail as follows.

Kandite, which includes kaolinite, halloysite, nacrite, and dickite,[26] is a class of common clay minerals existing in nature. Kaolinite, as a member of this kandite group, has a chemical structure that is different from that of montmorillonite. The layers of kaolinite [$Al_2Si_2O_5(OH)_4$] consist of a silicate tetrahedron and alumina octahedral arranged alternately at a ratio of 1:1 and connected into a lamellar packed structure by hydrogen

Additional Supporting Information may be found in the online version of this article

bonds and van der Waals forces.[27] In addition, the asymmetric structure of kaolinite originating from its crystal structure produces large superposed dipoles in the lamellar structure and, thus, a large cohesive energy.[26] This strong cohesive energy and low interlayer charge make it difficult for molecules, especially polymers, to intercalate into the interlaminar spaces of kaolinite.

As a facile, easily adopted, and greener chemical synthesis method, a mechanochemcial technique has been used to prepare various inorganic and organic materials.[28–35] In recent years, this method has been successfully extended to prepare inorganic–organic composite materials.[16,36–39] In this study, we used a novel pretreatment technology and a mechanochemical method to prepare an intercalated PANI–kaolinite nanocomposite through the *in situ* polymerization of aniline monomers in the presence of kaolinite clay. In addition, various characterization methods were used to study the structure, morphology, electrical conductivity, and thermal stability of the nanocomposite. The anticorrosive effect of the nanocomposite under a simulated marine environment was also preliminarily investigated.

EXPERIMENTAL

Reagents and Materials

Aniline, ammonium persulfate (APS), sodium chloride, and ethanol were purchased from Sinopharm Chemical Reagent Co., Ltd. These reagents were analytical grade. Superfine kaolinite (6000 mesh, 3.5 μm) was obtained from Aladdin. An epoxy resin emulsion (E571) and aqueous epoxy curing agent (8#) were purchased from Guangzhou Open Chemicals Co., Ltd. A defoamer free of volatile organic compounds and silicone (BYK-012) was obtained from BYK-Chemie GmbH. All of the materials and reagents were used as received without further purification.

Instrumental and Parameters

The X-ray diffraction patterns of the kaolinite, PANI, and intercalated PANI–kaolinite nanocomposite were obtained with an UltimaIV X-ray diffractometer (Rigaku, Japan). The IR spectra of the kaolinite, PANI, and nanocomposite were obtained with an iS10 Fourier transform infrared spectrometer (Nicolet) with a scanning range from 450 to 4000 cm^{-1} at a resolution of 4 cm^{-1}. The ultraviolet–visible spectra of PANI and the nanocomposite were obtained with a UV-2550 UV–visible spectrophotometer (Shimadzu, Japan) with a scanning range from 190 to 900 nm. The two samples were dispersed in distilled water by an ultrasonic treatment. The morphologies of the kaolinite, PANI, and nanocomposite were characterized by an S-3400N scanning electron microscope (Hitachi, Japan), HT-7700 transmission electron microscope (Hitachi, Japan), and Nanoscope Iva atomic force microscope (Veeco, Amercia), respectively. The electrical conductivity was measured with a KDY-1 four-probe electrical resistivity/sheet resistance tester (Kund Technology, China). The thermal stability was studied with a TG 209 F3 Tarsus thermogravimetric analyzer (Netzsch, Germany) in the temperature range from 20 to 820 °C at a heating rate of 20 °C/min under an argon atmosphere.

Preparation of the Intercalated PANI–Kaolinite Nanocomposite

An amount of 1 g of kaolinite was added to a 50-mL, round-bottomed flask. Then, the flask was sealed and vacuumed, and argon was charged into the flask 2–3 times followed by the addition of 2.5 mL of aniline with a 5-mL syringe according to the desired kaolinite–aniline mass ratio. The flask containing the raw materials was wrapped with silver paper and stored in the dark for 24 h. After that, the mixture was transferred into a mortar and was ground under an argon atmosphere with the gradual addition of APS. The amount of APS was determined according to various aniline–APS molar ratios of 1:1, 2:1, 3:1, 4:1, 5:1, 6:1, 1:2, 1:3, 1:4, 1:5, and 1:6. The reaction was finished when the mixture turned atropurpureus. The formed product was washed with distilled water and ethanol successively at least three times and filtered to remove unreacted APS, aniline, and some oligomers. The obtained filter cake was dried in a vacuum-drying oven at 40 °C for 24 h to obtain the intercalated PANI–kaolinite nanocomposite.

The process for preparing the pure PANI was similar to that used to prepare the intercalated PANI–kaolinite nanocomposite without the addition of kaolinite.

Anticorrosion Test of the Intercalated Nanocomposite

Preparation of the Coating of Epoxy Resin and the Intercalated PANI–Kaolinite Nanocomposite. Amounts of 1.4 g of epoxy resin emulsion and 0.1 g of the intercalated PANI–kaolinite nanocomposite were added to 1 mL of distilled water, and magnetic stirring was applied to the mixture solution to form a homogeneous solution. Then, 1.4 g of aqueous epoxy curing agent, 1 mL of deionized water, and two drops of BYK-012 defoamer were added to the mixed solution, respectively; this was followed by successive magnetic stirring and ultrasonic dispersion.

Epoxy resin coating for the blank test was prepared according to the process of epoxy resin/intercalated PANI–kaolinite nanocomposite coating without the addition of the nanocomposite.

Preparation of the A3 Steel Plate Coating. The as-prepared coatings were uniformly coated on A3 steel plates. The coated plates were preserved in an oven at 50 °C at least for 12 h to cure the epoxy resin.

Panel Experiment. The well-cured A3 steel plates were hung in simulated seawater containing 3.5 wt % sodium chloride, and the tracing observation of the corrosion changes of the A3 steel plates over time was performed.

RESULTS AND DISCUSSION

X-ray Diffraction Characterization of the Intercalated PANI–Kaolinite Nanocomposite

An intercalated PANI–kaolinite nanocomposite was prepared by the *in situ* polymerization of aniline monomers in the presence of kaolinite with a mechanochemical method. Figure 1 shows the typical X-ray powder patterns of the kaolinite, intercalated PANI–kaolinite nanocomposite, and PANI in the range 2–40°. As shown in Figure 1(a), we observed that there were four diffraction peaks located at 2θ positions of 12.5, 25.1, 35.2, and

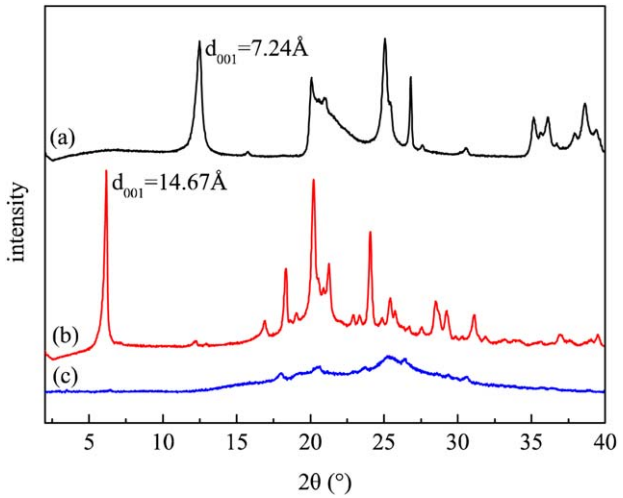

Figure 1. X-ray diffraction patterns of the (a) kaolinite, (b) intercalated PANI–kaolinite nanocomposite, and (c) PANI. [Color figure can be viewed in the online issue, which is available at wileyonlinelibrary.com.]

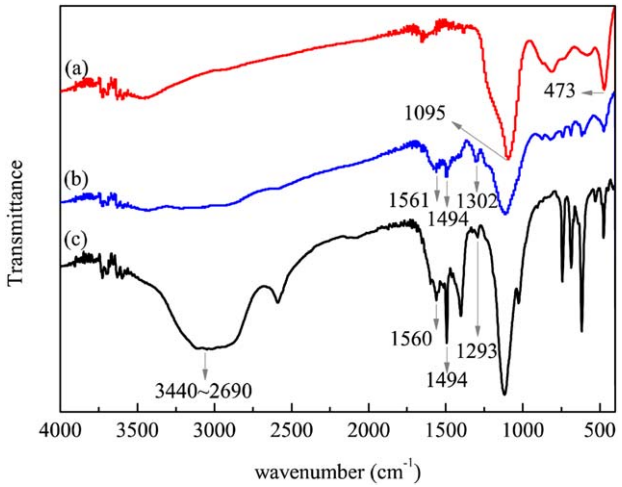

Figure 2. Fourier transform infrared spectra of the (a) kaolinite, (b) intercalated PANI–kaolinite nanocomposite, and (c) PANI. [Color figure can be viewed in the online issue, which is available at wileyonlinelibrary.com.]

38.3°; these were attributed to the crystalline structure of kaolinite.[40] The first peak at 12.5° related to the 001 plane corresponded to a basal spacing (d_{001}) of 7.24 Å. There were also two peaks correlated with quartz observed at 20.1 and 26.8°; this suggested the existence of quartz in the raw kaolinite.[40] The peaks at 17.9, 20.5, and 25.3° were caused by PANI [Figure 1(c)].[41] In the X-ray diffraction pattern of the intercalated PANI–kaolinite nanocomposite [Figure 1(b)], most of the diffraction peaks mentioned previously still appeared with little shifts to lower 2θ degrees. The diffraction peak attributed to the 001 plane in pristine kaolinite shifted to 6.2°; this corresponded to a d_{001} of 14.67 Å for the nanocomposite and resulted in a 7.43-Å expansion. The change in the *d*-spacing for kaolinite before and after the *in situ* mechanochemical polymerization was indicative of the intercalation of PANI chains in the interlamellar spaces of kaolinite[25,39,42] and, thus, demonstrated that PANI was successfully intercalated into the interlayers of kaolinite.

Fourier Transform IR and UV–Visible Spectra of the Intercalated PANI–Kaolinite Nanocomposite

Figure 2(a–c) presents the Fourier transform infrared spectra of the kaolinite, intercalated PANI–kaolinite nanocomposite, and PANI. The peaks at 1095 and 473 cm^{-1} in Figure 2(a) were assigned to the Si—O stretching vibrations and Si—O—Si characteristic vibrations of kaolinite,[43] respectively. In Figure 2(c), the two adjacent characteristic peaks at 1561 and 1494 cm^{-1} were assigned to the stretching vibrations of carbon–carbon double bonds from the quinonoid and benzenoid rings of PANI, respectively.[44] The peak at 1293 cm^{-1} was attributed to the C—N stretching vibrations of benzenoid units.[45,46] The wide absorption band at 3440–2690 cm^{-1} corresponded to the hydrogen-bonded N—H stretching vibrations (N—H...N) of intramolecular and intermolecular secondary amines.[47] As shown in Figure 2(b), the peaks mentioned previously still existed but with a significant decrease in the peak intensity when PANI was intercalated into kaolinite. This was because the steric hindrance effects from kaolinite might have limited the characteristic vibrations of the functional groups of PANI. Further analysis showed that the transmittance ratio of 1560:1494 cm^{-1} increased significantly without an obvious redshift or blueshift; this suggested that the content of quinonoid units or the oxidation degree of PANI in the nanocomposite was much higher than that in the neat PANI. In addition, the absorption peak of C—N of PANI showed a blueshift to 1302 cm^{-1} in the nanocomposite. We also found that the characteristic peaks of kaolinite (1750–1473 cm^{-1}) presented redshifts in the nanocomposite and partly overlapped with the peaks of PANI; this could be interpreted as the interaction between kaolinite and PANI. All this implied that PANI was intercalated into the interlayers of kaolinite.

The UV spectra of the PANI and intercalated PANI–kaolinite nanocomposite are recorded in Figure 3(a,b). Both spectra showed two peaks at about 230 nm (E band) and 280 nm (B band); these were assigned to the π–π* transition of benzene

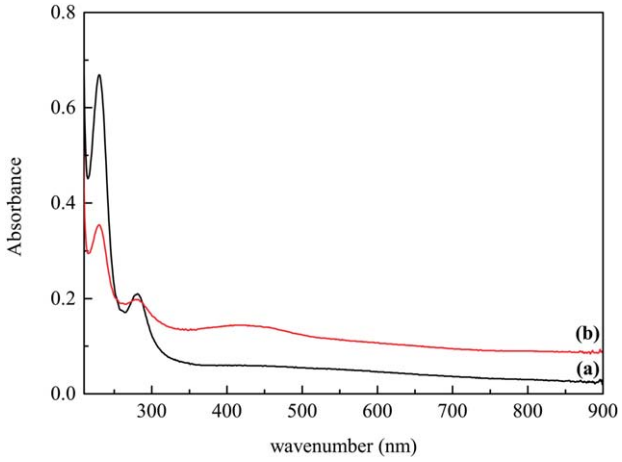

Figure 3. UV–visible spectra of the (a) PANI and (b) intercalated PANI–kaolinite nanocomposite dispersed in distilled water. [Color figure can be viewed in the online issue, which is available at wileyonlinelibrary.com.]

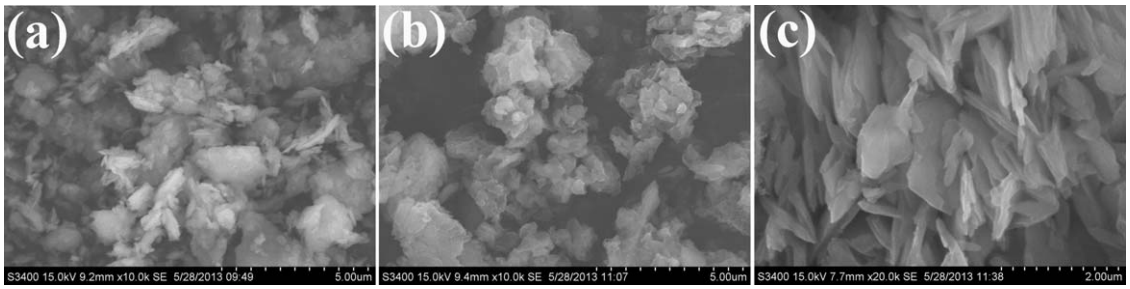

Figure 4. Scanning electron microscopy images of the (a) kaolinite, (b) intercalated PANI–kaolinite nanocomposite, and (c) PANI.

rings in the PANI chains. However, the peak of the nanocomposite at 280 nm was weaker and broader than that of PANI; this might have been due to interactions between the kaolinite and PANI. Interestingly, a weak absorption peak was observed around 430 nm in the UV–visible spectrum of the nanocomposite [Figure 3(b)], but it was not found in that of PANI [Figure 3(a)]. This peak was attributed to the p–π* transition of the quinonoid structure of PANI.[48] Therefore, the content of quinonoid units or the oxidation degree of PANI in the nanocomposite was higher than that in the neat PANI; this was in good agreement with the Fourier transform infrared results.

Morphological Characterization of the Intercalated PANI–Kaolinite Nanocomposite

The morphological characterization of the raw kaolinite, pristine PANI, and intercalated PANI–kaolinite nanocomposite was conducted by scanning electron microscopy, transmission electron microscopy, and atomic force microscopy, respectively. The surface morphology is shown in Figure 4. Kaolinite presented irregular particles with sizes of 1–3 μm and consisting of aggregates of kaolinite layers and also a few platelike structures [Figure 4(a)], whereas PANI exhibited a feathery or sheetlike structure [Figure 4(c)]. As shown in Figure 4(b), the nanocomposite was composed of anomalous three-dimensional cubes and basically retained the morphology of kaolinite. However, the evident difference was that kaolinite in the nanocomposite became expanded with some PANI sheets attached on the surface of the nanocomposite. Therefore, we inferred that the interlayer spacing of kaolinite was enlarged by polymer chains through intercalation effect of PANI; this was in good agreement with the X-ray diffraction analysis and Fourier transform infrared results.

To further confirm the successful synthesis of the intercalated nanocomposite, transmission electron microscopy observation with high resolution and higher magnifications was performed, as shown in Figure 5. Kaolinite gave a stacking lamellar structure consisting of regular polygons [Figure 5(a)], and PANI showed a nanofibrous morphology through the accumulation of PANI plates [Figure 5(c)]. Moreover, nanorods with a length of 100 nm and a diameter of 30 nm [Figure 5(b)] were observed in the nanocomposite; this demonstrated that kaolinite was intercalated with PANI. The schematic diagram of the intercalation process is shown in Figure 6.

Atomic force microscopy pictures of the kaolinite/PANI blending mixture and intercalated PANI–kaolinite nanocomposite are shown in Figure 7. Through a comparison of Figures 7(a) and 7(b), we found that the kaolinite and PANI of the intercalated PANI–kaolinite nanocomposite were well-distributed without obvious phase interfaces, whereas the two components of the blending mixture behaved in the opposite manner. This was because the former achieved a more uniform combination by intercalation, whereas the latter was just macromixed.

Electrical Conductivity of the Intercalated PANI–Kaolinite Nanocomposite

The relationship between the electrical conductivity and intercalation effects is summarized in Table 1. The results suggest that PANI was successfully intercalated into the interlayers of kaolinite in an aniline–APS molar ratio of 2:1 or 1:1. The electrical conductivity values had the same order of magnitude as those measured in a previous study,[49] which reported a conducting PANI–kaolinite composite synthesized by *in situ* oxidative polymerization in the presence of kaolinite in an aqueous solution.

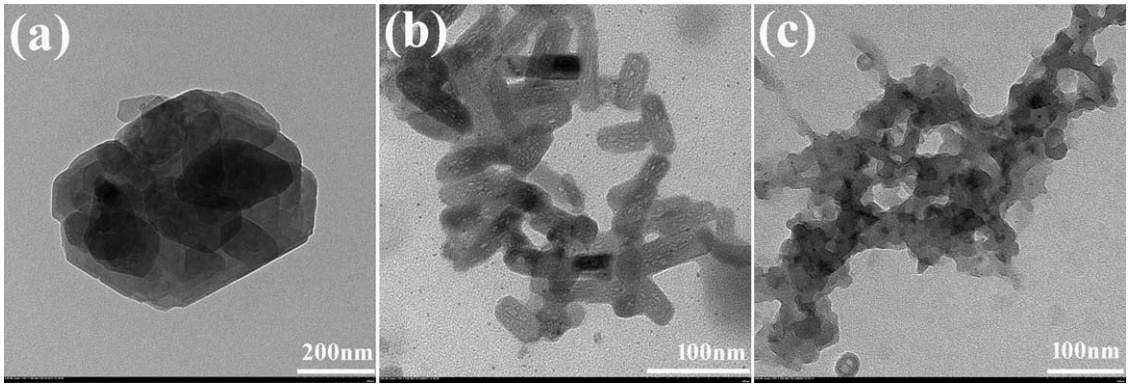

Figure 5. Transmission electron microscopy photographs of the (a) kaolinite, (b) intercalated PANI–kaolinite nanocomposite, and (c) PANI.

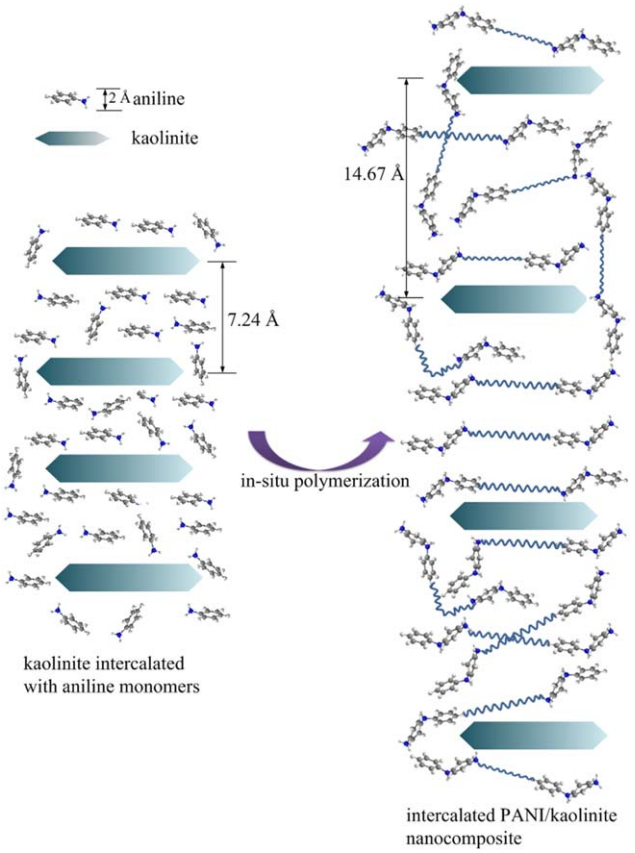

Figure 6. Schematic diagram of the intercalation process. [Color figure can be viewed in the online issue, which is available at wileyonlinelibrary.com.]

There was a trend in which d_{001} of kaolinite in the nanocomposite increased with decreasing amount of APS when then amount of aniline remained constant. On the other hand, the nanocomposite showed a higher electrical conductivity in a lower amount of APS. Therefore, we inferred that a bigger d_{001} or better intercalation effect of the nanocomposite led to a higher electrical conductivity.

Thermogravimetric Analysis

The thermogravimetric curves of the raw kaolinite, intercalated PANI–kaolinite nanocomposite, and pristine PANI are shown in Figure 8. The molar ratio of aniline to APS was 1:1 in the raw

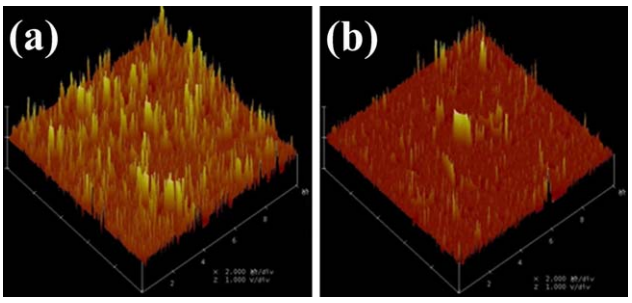

Figure 7. Atomic force microscopy pictures of the (a) intercalated PANI–kaolinite nanocomposite and (b) kaolinite/PANI mixture. [Color figure can be viewed in the online issue, which is available at wileyonlinelibrary.com.]

Table 1. Relationship Between the Conductivity and Intercalation Effects of the Nanocomposite

$n_{aniline}/n_{APS}$[a]	$m_{kaolinite}$[b] (g)	$V_{aniline}$[c] (mL)	K[d] (10^{-3} S cm^{-1})	d_{001} (Å)
2:1	1.00	2.5	8.0	14.47
1:3	1.00	2.5	—	—
1:1	1.00	2.5	1.6	14.19

[a] $n_{aniline}/n_{APS}$: molar ratio.
[b] $m_{kaolinite}$: the mass of kaolinite.
[c] $V_{aniline}$: the volume of aniline.
[d] K: electrical conductivity.

materials for the nanocomposite and PANI. The weight of kaolinite almost remained invariant, even when the temperature increased to 750 °C [Figure 8(a)]. As shown in Figure 8(c), we observed that the weight loss of PANI experienced two stages. The first stage, below 200 °C, resulted from the desorption of absorbed water, and the second stage, from 200 to 370 °C, was attributed to the thermal decomposition of the backbones of PANI. After that, the weight of the decomposed PANI just underwent a slight decrease, reaching a weight loss of 80% at 750 °C. However, when PANI was intercalated into kaolinite by *in situ* polymerization, the weight loss was obviously decreased [Figure 8(b)]. Concretely, the weight loss of the nanocomposite mainly occurred below 350 °C; this could be interpreted as the desorption of absorbed water. Here, the existence of kaolinite in the nanocomposite hindered the desorption of absorbed water, and the whole process was finished until the temperature reached 350 °C. When the temperature was higher than 350 °C, the weight of the nanocomposite decreased slightly, and even at 750 °C, there was still 60% residue left. Therefore, the thermal stability of PANI in the nanocomposite was significantly improved compared with that of pristine PANI. This result indicates that PANI was intercalated into the kaolinite interlayers, and this was in excellent accordance with previous characterization results. In addition, the thermogravimetric curves of the

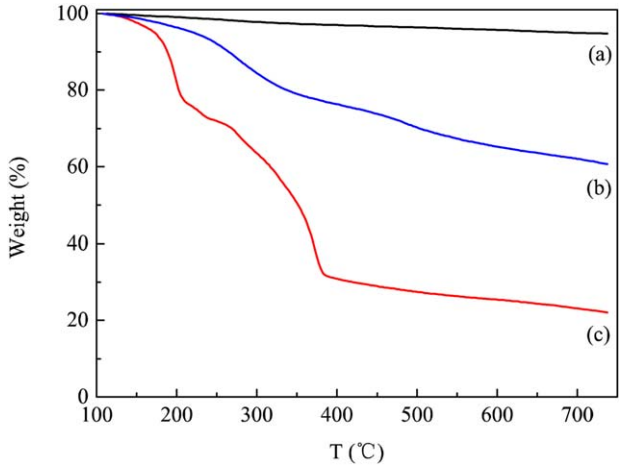

Figure 8. Thermogravimetric curves of the (a) kaolinite, (b) intercalated PANI–kaolinite nanocomposite, and (c) PANI (T = temperature). [Color figure can be viewed in the online issue, which is available at wileyonlinelibrary.com.]

intercalated PANI–kaolinite nanocomposite with different aniline–APS molar ratios are summarized in Figure S1 (see Supporting Information), from which we found that the nanocomposite was most thermally stable at a 1:2 aniline–APS molar ratio.

Anticorrosion Evaluation

It has been reported that PANI/montmorillonite composites show better anticorrosive effects,[50,51] so we were concerned with whether the intercalated PANI–kaolinite nanocomposite would show similar behavior. To investigate the anticorrosive effects of the epoxy resin/intercalated PANI–kaolinite nanocomposite coating on an A3 steel plate under a seawater environment, a series of anticorrosion tests in simulated seawater were performed, and the results are recorded in Figure S2 (see Supporting Information). For the convenience of a performance comparison, a blank test for the neat epoxy-coated A3 steel plate was also conducted. A3 steel plates coated with epoxy resin in the absence and presence of the intercalated PANI–kaolinite nanocomposite were immersed in simulated seawater for 19 days, and their corrosion changes over time were investigated. We found that no obvious corrosion was observed in either of the A3 steel plates [Figure S2(b,f)] at 3 days. After 9 days, the A3 steel plate coated with the epoxy resin coating was significantly corroded [Figure S2(c)], whereas the plate coated with epoxy resin/intercalated PANI–kaolinite nanocomposite was slightly eroded on the edge area [Figure S2(g)]; this was probably caused by uneven coating. After 19 days, the former was seriously rusted [Figure S2(d)], whereas the latter was only slightly corroded [Figure S2(h)]. The previous results suggest that the epoxy resin/intercalated PANI–kaolinite nanocomposite coating had a better anticorrosive effect than that common epoxy resin coating under a simulated marine environment.

CONCLUSIONS

A novel pretreatment technology and environmentally friendly mechanochemical polymerization were used to prepare an intercalated PANI–kaolinite nanocomposite. Results from various characterization methods reveal that PANI was successfully intercalated into the interlamellar spaces of kaolinite via *in situ* polymerization. We found that the intercalated PANI–kaolinite nanocomposite had more excellent thermal stability compared with neat PANI. The epoxy resin coating with the presence of the nanocomposite achieved a better anticorrosive effect than that without the composite under simulated seawater conditions. The obtained target nanocomposite has a potential advantage in the field of marine anticorrosion in the near future.

ACKNOWLEDGMENTS

This work was financially supported by the Key Laboratory of Marine Ecosystem and Biogeochemistry of the State Oceanic Administration (contract grant number LMEB201403) and the Public Science and Technology Research Program Foundation of Ocean (contract grant number 201405036-3). This work was also supported by the National Science Foundation of China (contract grant number 91128212).

REFERENCES

1. Xie, J. X.; Han, X.; Zong, C. Y.; Ji, H. P.; Lu, C. H. *Macromolecules* **2015**, *48*, 663.
2. Du, X. F.; Xu, Y. L.; Xiong, L. L.; Bai, Y.; Zhu, J. B.; Mao, S. C. *J. Appl. Polym. Sci.* **2014**, *131*, DOI: 10.1002/app.40827.
3. Sanches, E. A.; da Silva, J. M. S.; Ferreira, J. M. D.; Soares, J. C.; dos Santos, A. L.; Trovati, G.; Fernandes, E. G. R.; Mascarenhas, Y. P. *J. Mol. Struct.* **2014**, 1074, 732.
4. Marcasuzaa, P.; Reynaud, S.; Ehrenfeld, F.; Khoukh, A.; Desbrieres, J. *Biomacromolecules* **2010**, *11*, 1684.
5. Armelin, E.; Alemán, C.; Iribarren, J. *I. Prog. Org. Coat.* **2009**, *65*, 88.
6. Arefinia, R.; Shojaei, A.; Shariatpanahi, H.; Neshati, J. *Prog. Org. Coat.* **2012**, *75*, 502.
7. Ma, S. D.; Song, G. L.; Feng, N. B.; Zhao, P. *J. Appl. Polym. Sci.* **2012**, *125*, 1601.
8. Yeh, J. M.; Liou, S. J.; Lai, C. Y.; Wu, P. C. *Chem. Mater.* **2001**, *13*, 1131.
9. Navarchian, A. H.; Joulazadeh, M.; Karimi, F. *Prog. Org. Coat.* **2014**, *77*, 347.
10. Binitha, N. N.; Sugunan, S. *J. Appl. Polym. Sci.* **2008**, *107*, 3367.
11. Tokarský, J.; Kulhánková, L.; Neuwirthová, L.; Mamulová Kutláková, K.; Vallová, S.; Stýskala, V.; Čapková, P. *Mater. Res. Bull.* **2016**, *75*, 139.
12. Liu, Y. S.; Liu, Y. Z.; Jiang, X. Q.; Liu, T. Z.; Yan, X. S.; Fan, Y. F.; Cai, Q.; Zhang, J. M.; Zhang, L. X. *Polym. Compos.* **2015**, *36*, 1759.
13. Jun, C. S.; Sim, B.; Choi, H. *J. Colloids Surf. A* **2015**, *482*, 670.
14. Chae, H. S.; Zhang, W. L.; Piao, S. H.; Choi, H. *J. Appl. Clay Sci.* **2015**, *107*, 165.
15. Li, S.; Wei, Y.; Kong, Y.; Tao, Y. X.; Yao, C.; Zhou, R. H. *Synth. Met.* **2015**, *199*, 45.
16. Yoshimoto, S.; Ohashi, F.; Ohnishi, Y.; Nonami, T. *Synth. Met.* **2004**, *145*, 265.
17. Kim, B. H.; Jung, J. H.; Hong, S. H.; Kim, J. W.; Choi, H. J.; Joo, J. *Curr. Appl. Phys.* **2001**, *1*, 112.
18. Azhar, F. F.; Olad, A.; Mirmohseni, A. *Polym. Bull.* **2014**, *71*, 1591.
19. Toumi, I.; Benyoucef, A.; Yahiaoui, A.; Quijada, C.; Morallon, E. *J. Alloys Compd.* **2013**, *551*, 212.
20. Kulhánková, L.; Tokarský, J.; Peikertová, P.; Mamulová Kutláková, K.; Ivánek, L.; Čapková, P. J. *Phys. Chem. Solids* **2012**, *73*, 1530.
21. Ma, J. Z.; Gao, D.; Lü, B.; Chu, Y.; Dai, J. F. *Mater. Manuf. Processes* **2007**, *22*, 715.
22. Zeng, Q. H.; Wang, D. Z.; Yu, A. B.; Lu, G. Q. *Nanotechnology* **2002**, *13*, 549.
23. Song, D. H.; Lee, H. M.; Lee, K. H.; Choi, H. J. *J. Phys. Chem. Solids* **2008**, *69*, 1383.
24. Wang, B. X.; Liu, C. J.; Yin, Y. C.; Tian, X. L.; Yu, S. S.; Chen, K. Z.; Liu, P. B.; Liang, B. *J. Appl. Polym. Sci.* **2013**, *130*, 1104.

25. Elbokl, T. A.; Detellier, C. *J. Phys. Chem. Solids* **2006**, *67*, 950.
26. Chakraborty, C.; Sukul, P. K.; Dana, K.; Malik, S. *Ind. Eng. Chem. Res.* **2013**, *52*, 6722.
27. White, C. E.; Kearley, G. J.; Provis, J. L.; Riley, D. P. *J. Chem. Phys.* **2013**, *138*, 194501.
28. Nenadović, S. S.; Kljajević, L. M.; Nenadović, M. T.; Mirković, M. M.; Marković, S. B.; Rakočević, Z. L. *Environ. Earth Sci.* **2015**, *73*, 7669.
29. Badapanda, T.; Sarangi, S.; Parida, S.; Behera, B.; Ojha, B.; Anwar, S. *J. Mater. Sci. Mater. Electron.* **2015**, *26*, 3069.
30. Clarke, T. J.; Davies, T. E.; Kondrat, S. A.; Taylor, S. H. *Appl. Catal. B* **2015**, *165*, 222.
31. Rak, M. J.; Friscic, T.; Moores, A. *Faraday Discuss.* **2014**, *170*, 155.
32. Rajput, L.; Banerjee, R. *Cryst. Growth Des.* **2014**, *14*, 2729.
33. Ravnsbæk, J. B.; Swager, T. M. *ACS Macro Lett.* **2014**, *3*, 305.
34. Zhang, Y.; Jamal, R.; Shao, W. W.; Abdiryim, T. *Electrochim. Acta* **2013**, *113*, 382.
35. Yoshimoto, S.; Ohashi, F.; Kameyama, T. *Macromol. Rapid Commun.* **2004**, *25*, 1687.
36. Palaniappan, S.; Chang, Y. T.; Liu, C. M.; Manisankar, P. *J. Appl. Polym. Sci.* **2012**, *124*, 4281.
37. Matoga, D.; Oszajca, M.; Molenda, M. *Chem. Commun.* **2015**, *51*, 7637.
38. Masoomi, M. Y.; Morsali, A.; Junk, P. C. *CrystEngComm* **2015**, *17*, 686.
39. Wu, C. S.; Huang, Y. J.; Hsieh, T. H.; Huang, P. T.; Hsieh, B. Z.; Han, Y. K.; Ho, K. S. *J. Polym. Sci. Part A: Polym. Chem.* **2008**, *46*, 1800.
40. Vilela, S. O.; Soto-Oviedo, M. A.; Albers, A. P. F.; Faez, R. *Mater. Res.* **2007**, *10*, 297.
41. Posudievsky, O. Y.; Goncharuk, O. A.; Barille, R.; Pokhodenko, V. D. *Synth. Met.* **2010**, *160*, 462.
42. Abd El-Ghaffar, M. A.; Youssef, A. M.; Abd El-Hakim, A. A. *Arab. J. Chem.* **2015**, *8*, 771.
43. Spence, A.; Kelleher, B. P. *Vib. Spectrosc.* **2012**, *61*, 151.
44. Arasi, A. Y.; Jeyakumari, J. J. L.; Sundaresan, B.; Dhanalakshmi, V.; Anbarasan, R. *Spectrochim. Acta A* **2009**, *74*, 1229.
45. Ye, J. R.; Zhai, S.; Gu, Z. J.; Wang, N.; Wang, H.; Shen, Q. *Mater. Lett.* **2014**, *132*, 377.
46. Ginic-Markovic, M.; Matisons, J. G.; Cervini, R.; Simon, G. P.; Fredericks, P. *M. Chem. Mater.* **2006**, *18*, 6258.
47. Trchová, M.; Šeděnková, I.; Konyushenko, E. N.; Stejskal, J.; Holler, P.; Ćirić-Marjanović, G. *J. Phys. Chem. B* **2006**, *110*, 9461.
48. Yoshimoto, S.; Ohashi, F.; Kameyama, T. *J. Polym. Sci. Part B: Polym. Phys.* **2005**, *43*, 2705.
49. Duran, N. G.; Karakışla, M.; Aksu, L.; Saçak, M. *Mater. Chem. Phys.* **2009**, *118*, 93.
50. Bagherzadeh, M.; Ghasemi, M. *J. Pet. Sci. Eng.* **2015**, *5*, 1.
51. Mousavinejad, T.; Bagherzadeh, M. R.; Akbarinezhad, E.; Ahmadi, M.; Guinel, M. *J. F. Prog. Org. Coat.* **2015**, *79*, 90.

SGML and CITI Use Only
DO NOT PRINT